

Article

Geochemical Characteristics of Chlorite in Xiangshan Uranium Ore Field, South China and Its Exploration Implication

Yongjian Wang , Honghai Fan , Yaqing Pang and Wei Xiao

Beijing Research Institute of Uranium Geology, China National Nuclear Corporation, Beijing 100029, China; pang_82@eyou.com (Y.P.); xiaowei2879@126.com (W.X.)

* Correspondence: wangyongjianhao123@163.com (Y.W.); fhh270@263.net (H.F.); Tel.: +86-6496-4924 (Y.W.); +86-6496-0709 (H.F.)

Abstract: Chlorite is one of the most important hydrothermal minerals in many hydrothermal uranium deposits worldwide and is commonly closely associated with the uranium mineralization. Trace elements in chlorite have been extensively applied to fingerprinting the hydrothermal fluid evolution and indicating the concealed ore bodies in porphyry Cu (-Au) deposits and skarn-related Pb-Zn deposits. However, this approach was rarely attempted on hydrothermal uranium deposits to date. Xiangshan uranium ore field, located in the southeast part of Gan-Hang Metallogenic (or Volcanic) Belt (GHMB), is the largest volcanic-related ore field in the whole country. In this study, the focus was placed on the petrographic characteristics and trace elements in hydrothermal chlorite from two typical deposits (Zoujiashan and Yunji) at Xiangshan. Four types of chlorites were identified, i.e., Chl1-Y and Chl2 from Yunji deposit, and Chl1-Z and Chl3 from Zoujiashan deposit. The pre-ore Chl1-Y and Chl1-Z are formed through replacing the original magmatic biotite. Chl2 and Chl3 occur as veinlets or disseminated, and are closely associated with early-ore U mineralization and main-ore U mineralization, respectively. All the four types of chlorites are typically trioctahedral chlorite. Vein-type/disseminated Chl2 and Chl3 in ore veins were precipitated directly from the hydrothermal fluids through dissolution-migration-precipitation mechanism, whereas the replacement-type chlorite was formed by the dissolution-crystallization mechanism. Empirical geothermometry indicates that the chlorite from Yunji and Zoujiashan were crystallized at 179~277 °C, indicating a mesothermal-epithermal precipitation environment. EPMA and LA-ICP-MS results show that the replacement-type chlorite has relatively consistent compositions at Yunji and Zoujiashan. Both Chl2 and Chl3 are enriched in U, Th but depleted in Mn and Ti. Compared with the Chl2 related to early-ore U mineralization, Chl3 that formed at main-ore stage has higher concentrations of Fe, U, Th, REEs, Mn and Ti, as well as higher Fe/(Fe + Mg) ratios. Such compositional differences between Chl2 and Chl3 are mainly attributed to the formation temperatures and fluid compositions/natures. Combined with petrology and chemical compositions of different types of chlorite, we propose that the presence of vein-type/disseminated chlorite with high U and Fe/(Fe + Mg) ratio but relatively low Mn, Ti and Pb contents can be regarded as an effective vector toward the most economic (high U grade) mineralized zone, whereas the occurrence of Chl2 is likely to indicate the subeconomic U mineralization and less potential exploration for uranium at depth.

Keywords: chlorite chemistry; geothermometry; LA-ICP-MS; exploration; Xiangshan uranium ore field



Citation: Wang, Y.; Fan, H.; Pang, Y.; Xiao, W. Geochemical Characteristics of Chlorite in Xiangshan Uranium Ore Field, South China and Its Exploration Implication. *Minerals* **2022**, *12*, 693. <https://doi.org/10.3390/min12060693>

Academic Editors: Kunfeng Qiu, Callum Hetherington and Antonio Simonetti

Received: 11 March 2022

Accepted: 27 May 2022

Published: 30 May 2022

Publisher's Note: MDPI stays neutral with regard to jurisdictional claims in published maps and institutional affiliations.



Copyright: © 2022 by the authors. Licensee MDPI, Basel, Switzerland. This article is an open access article distributed under the terms and conditions of the Creative Commons Attribution (CC BY) license (<https://creativecommons.org/licenses/by/4.0/>).

1. Introduction

Chlorite mineral group (Mg, Fe²⁺, Fe³⁺, Mn, Al)₁₂[(Si, Al)₈O₂₀](OH)₁₆ comprises the most common phyllosilicates in nature, and can form during sedimentary, metamorphic, and magmatic-hydrothermal processes [1,2]; for simplicity, it will be hereafter referred to as a mineral. In most of the magmatic-hydrothermal systems, chlorite is closely associated

with the formation of some deposits, such as in porphyry-related Cu-Au deposits [3–8], volcanogenic massive sulfide (VMS) Zn-Pb deposits [9], orogenic Au deposits [10–12], skarn Fe-Cu deposits [13,14], and hydrothermal U (Th) deposits [15–23]. Chlorite commonly exhibits a wide range of variations in crystallochemical and chemical compositions, hinging on the bulk rock composition and physicochemical conditions at the formation [24]. For instance, Cathelineau and Nieva [25] found good linear relations between temperatures and concentrations of Fe, Mg, Al^{iv} in chlorite. Some researchers also found that the chemical compositions in chlorite show correlations with sulfur fugacity and oxygen fugacity during the crystallization of chlorite [26–29]. Therefore, chlorite has been widely used as a very effective geothermometer to calculate the temperature of ore formation [30,31] and as a vector mineral to trace the fluid evolution [32–34]. A total of four approaches to chlorite geothermometry have been proposed in the past few decades, including structural, empirical, thermodynamic and semi-empirical, of which the empirical and semi-empirical methods were mostly used in ore deposit studies ([31], and reference therein). More recently, the spatial variation of trace elements in chlorite was utilized to fingerprint the hydrothermal center or concealed orebodies of the porphyry-related and skarn-related deposits [3–5,14]. Because chlorite is also widely found in most of the hydrothermal uranium deposits [15–23], the studies on chemical variation of chlorite in these U deposits may provide some new insights into the ore fluids evolution and ore prospecting implications. However, the characterization on the trace elements of chlorite were rarely reported for hydrothermal uranium deposits to date.

The Xiangshan uranium ore field, located in the northeastern part of Gan-Hang Metallogenic Belt (hereafter referred to as the GHMB), is the largest volcanic-related uranium ore field in China with a proven metal reserves of 26,000 t U [35,36]. An abundance of gangue minerals (e.g., chlorite, fluorite, calcite) are widely developed in most of the discovered U deposits and are closely associated with uranium mineralization. The chlorite and illite alteration are mostly developed in the host rocks and ore bodies. In addition, the wall-rock alteration commonly shows both vertical and lateral variations [37,38]. As such, the compositional variations of the widespread chlorite may potentially serve as the vector mineral to reflect the nature and evolution of ore-forming fluids and indicate the concealed U mineralization.

In this contribution, we collected the samples from two typical uranium deposits (Zoujiashan and Yunji deposits) at Xiangshan. Based on the field geological surveys and detailed microscopic observations, we performed the EPMA and LA-ICP-MS analyses for different types of chlorite from the two deposits, with the aim to discuss the chemical compositions and origin of chlorites, and their implications for uranium ore exploration.

2. Geological Setting

The Gan-Hang Metallogenic (or Volcanic) Belt is the most important volcanic-related uranium ore belt which hosts a number of U deposits with tonnage of >3000 t U. Tectonically, the GHMB is localized on the southwestern part of the Jiang-Shao Suture Zone [39–41], a giant collisional zone which spatially separates the Yangtze and Cathaysia blocks [42,43] (Figure 1a). The GHMB extends along the Jiangshan-Shaoxing suture and starts from Yongfeng in Jiangxi Province to the Shaoxing in Zhejiang Province. The exposed stratigraphy of the GHMB mainly includes the Precambrian metamorphic rocks, Mesozoic volcanics/granitoids and Cretaceous terrestrial clastics [39]. From southwest to northeast, three major uranium ore fields, i.e., Xiangshan, Shengyuan and Dazhou, are present within three fault-controlled volcanic basins of the GHMB. In addition to uranium, these volcanic basins also abound in copper, gold, silver, lead and zinc resources [41,44].

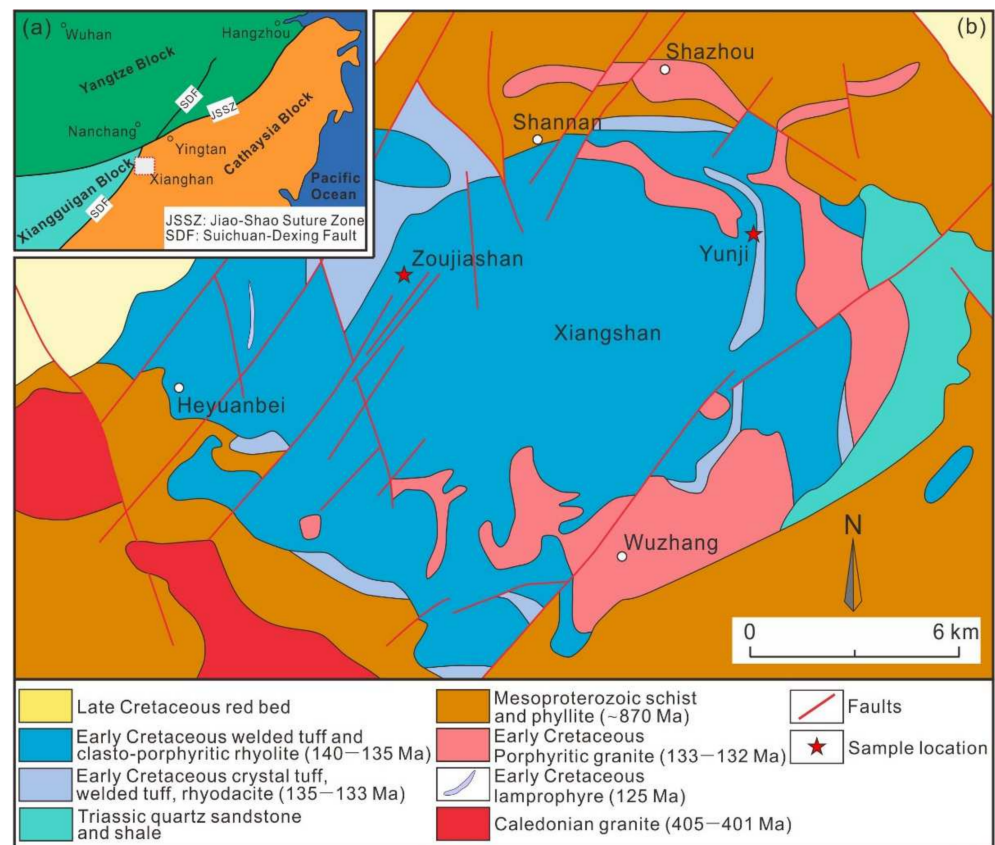


Figure 1. (a) Sketched map showing the location of the Xiangshan uranium ore field in South China; (b) Simplified geological map of Xiangshan uranium ore field showing the location of Zoujiashan deposit and Yunji deposit investigated in this study (modified after Lin et al. [37]).

As the largest volcanic-related uranium deposits in China, the Xiangshan ore field hosts a total of twenty-six uranium deposits associated with the early Cretaceous intermediate-felsic magmatism [37,45] (Figure 1b). The large-scale magmatic eruption, effusion and intrusion resulted in the formation of a volcanic-intrusive complex which comprises a resurgent caldera. The exposed stratigraphy in the study area mainly consists of the Mesoproterozoic metamorphic rocks, Lower Carboniferous and Upper Triassic metasedimentary rocks and early Cretaceous volcanic rocks (Figure 1b). The metamorphic rocks are widespread in the region and mainly comprise phyllites, schists and amphibolites with metamorphic grade ranging from lower greenschist to lower amphibolite facies. There are basically two volcanic formations which are separated by intermittent pyroclastic rocks (e.g., tuff, tuffaceous sandstone) [46–48]. The lower Daguding Fm. volcanics are mainly composed of rhyodacite and minor rhyolitic crystal tuff, ignimbrite, whereas the upper Ehuling Fm. volcanics primarily consist of porphyritic lava which is the most voluminous volcanic rock in Xiangshan. Recent work on the zircon U-Pb geochronology indicated that these (sub) volcanic rocks were emplaced within a very short period (ca.137–132 Ma) [49,50]. The western parts of the Xiangshan volcanic basin were covered by the Cretaceous red clastic sedimentary rocks which are composed of marls and evaporites (gypsum) [42,44].

Most of the discovered uranium deposits are regionally controlled by NE-trending faults. The majority of uranium ore bodies are predominately hosted by the volcanic (subvolcanic) rocks. Based on the mineral assemblages and crosscutting relationships, two important episodes of uranium mineralization have been distinguished in the Xiangshan ore field, i.e., the early ore stage (alkali metasomatic U mineralization) with subeconomic U mineralization and the main ore stage (acidic metasomatic U-Th mineralization) [36,45,51]. The uranium mineralization of early ore stage is predominately characterized by albite-hematite-chlorite assemblages, whereas the main ore stage is featured by abundant pitch-

blende, fluorite and illite. The pitchblende-fluorite-illite veins (main ore stage) commonly overlap with the red-colored mineralized body (early ore stage).

3. Ore Deposit Geology and Hydrothermal Alteration

3.1. Ore Deposit Geology

The Zoujiashan U-Th deposit is situated in the western Xiangshan caldera. The ore reserves in the Zoujiashan mining area exceeds over U 10,000 t [52]. The major exposed sequences are the Ehuling Fm. porphyritic lava (Figure 1b). From the surface down, the strata in this deposit are mainly composed of porphyritic lava, rhyodacite and ignimbrite, as well as Mesoproterozoic quartz schist (Figure 2a). The metamorphic rocks are mainly distributed at depths of <1000 m. The main minerals of unaltered volcanic rocks are intermediate-felsic in composition and mainly include plagioclase, K-feldspar, quartz and biotite. The uranium ore bodies of the Zoujiashan are mainly hosted in the rhyodacite and porphyritic lava (Figure 2a). Only a minor proportion of orebodies are hosted in the pyroclastic rocks. The spatial location of the ore bodies is rigidly controlled by the NE-oriented Zoujiashan-Shidong Fault and its subordinated NNE-, NS- and NNW-oriented faults, and hosted by the altered fractured volcanic rocks. There are numerous ore bodies with different sizes. The ore bodies commonly occur as lenses or veins with 50–150 m in length, 20–100 m in width and 1–3 m in thickness [51]. The uranium grades of the ores generally range from 0.1% to 0.5%, with an average of 0.3%. The most important metallic minerals include thorium-bearing pitchblende, brannerite and coffinite, along with minor thorite, pyrite, galena and molybdenite. Gangue minerals include illite, fluorite, calcite and clay minerals (Figure 3).

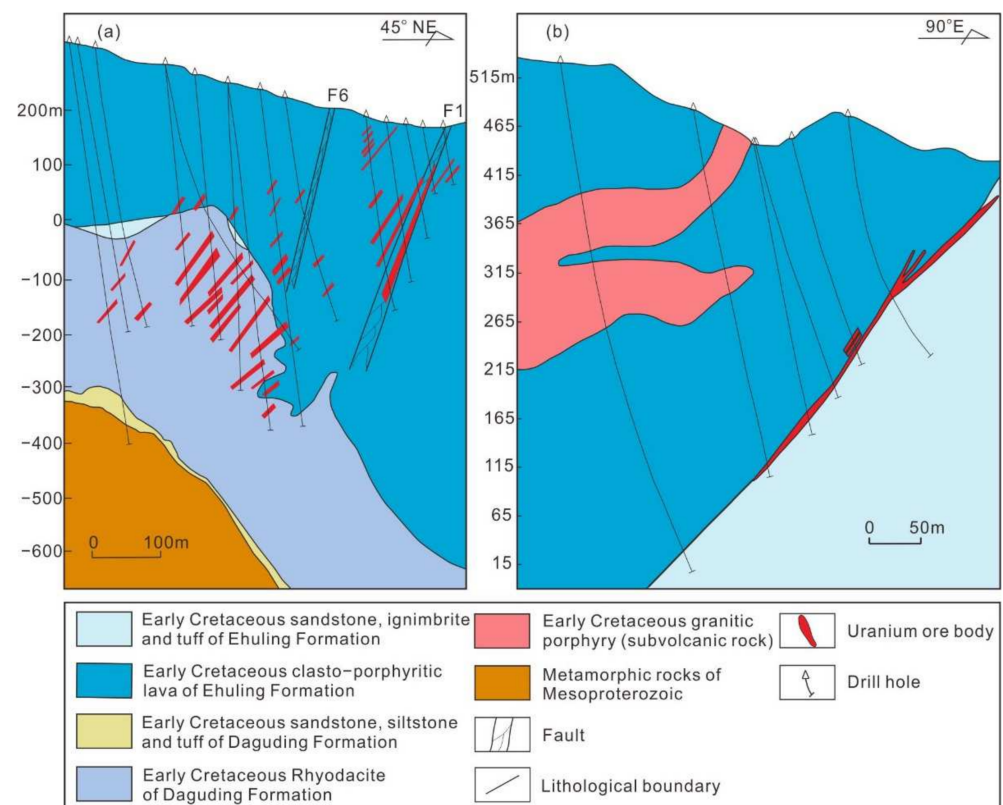


Figure 2. Typical geologic profiles for uranium prospecting at Zoujiashan deposit (a) and Yunji deposit (b) (modified from Zoujiashan and Yunji exploration reports).

Minerals	Pre-ore stage	Syn-ore stage		Post-ore stage
		Early ore stage	Main ore stage	
Illite	—————		—————	-----
Albite	—————			
Chlorite	Chl1 —————	Chl2 —————	Chl3 —————	
Carbonate		—————		-----
Quartz				
Apatite		—————	—————	
Hematite		—————		
Fluorite			—————	-----
Pyrite			—————	
Galena			—————	
Sphalerite			—————	
Chalcopyrite			—————	
Molybdenite			—————	
Arsenopyrite			—————	
Brannerite		—————	—————	
Coffinite		—————	—————	
Thorite			-----	
Uranothorite			—————	
Pitchblende		—————	—————	
Xenotime			-----	

Figure 3. Paragenetic sequence of altered and ore minerals at Xiangshan uranium ore field.

The Yunji deposit is located in the northern part of the Xiangshan caldera and contains >1000 t U ores with an average grade of 0.1% [52]. The Yunji deposit is the only one where alkali metasomatic U mineralization (subeconomic) is predominated. The exposed strata of the deposit are the Ehuling Fm. porphyritic lava, tuffaceous sandstone and ignimbrite, and the uranium ore bodies are mainly hosted by the porphyritic lava (Figure 2b). The granitic porphyry occurs as dykes at the depth of the deposit, intruding into the porphyritic lava. The granitic porphyry has the similar compositions with rhyolite and porphyritic lava. The ore bodies are strictly controlled by a near NS-trending arc-like fault and mainly distributed along the subordinated fractures. The major ore bodies extend stably, with large veins being 45 m in width and 2 m in thickness. In contrast, some small ore veins are lenticular with limited length and thickness. Because the development of fractures in Yunji are not abundant as those in Zoujiashan, the ore bodies in the two ore deposits have different morphology and size. The mineralogy of the Yunji deposit is also distinguishable from that of the Zoujiashan. In comparison with the Zoujiashan deposit, albite and hematite (typical altered minerals of alkali metasomatic U mineralization) are abundant and extensively distributed, and horizontal zoning of alteration is also widespread and unequivocal. The main uranium minerals include brannerite, U-Ti phases and coffinite, along with minor galena and sphalerite. Gangue minerals include albite, hematite, calcite, chlorite and apatite (Figure 3).

3.2. Alteration Paragenesis

Chloritization is one of the most extensive alteration types at Xiangshan. At Yunji, two chlorite types have been identified based on their spatial distribution, morphology and paragenesis, i.e., Chl1-Y and Chl2 [18]. Chl1-Y is partially or totally altered from igneous biotite and closely associated with pre-ore alteration. Chl1-Y alteration occurs pervasively in both proximal and distal parts of the ore body and generally can extend over tens of meters. The associated pre-ore minerals are albite and calcite. Chl2 predominately occurs as disseminated aggregates or veinlets in the center of the ore bodies and is genetically associated with alkali metasomatic U mineralization. The Chl2 was commonly observed to coexist with U minerals (Figure 4e,f). Alteration mineral assemblage for Chl2 stage is composed of chlorite, calcite, apatite, and hematite (Figures 3 and 4e,f).

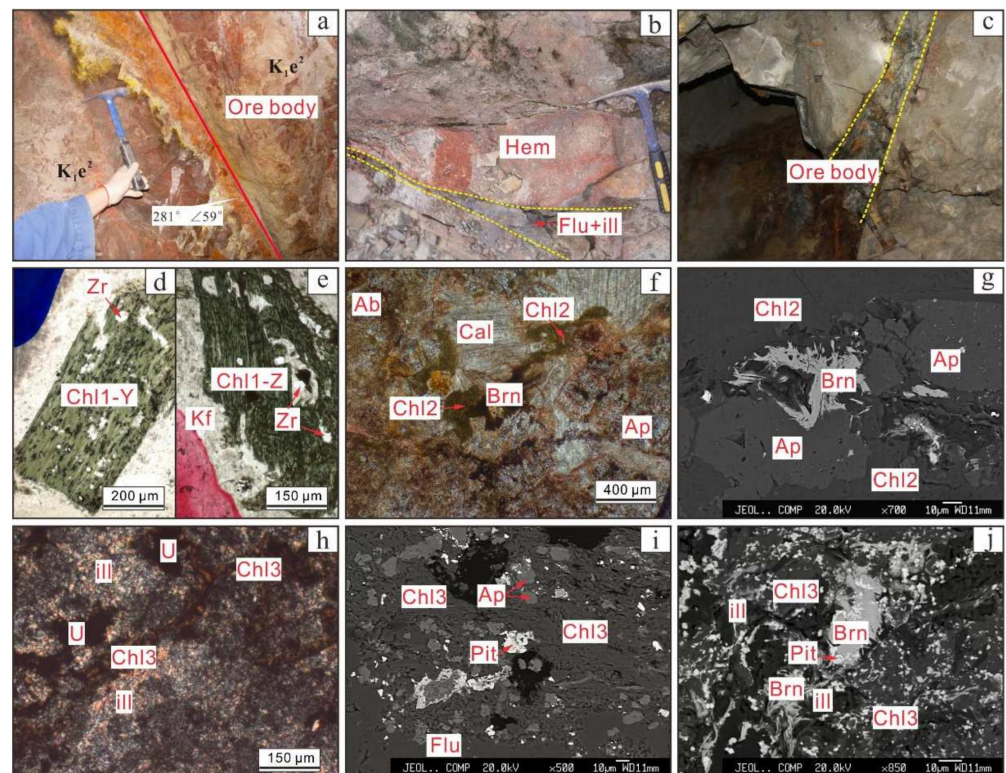


Figure 4. Photographs of typical uranium ore body and micrographs of typical chlorite alteration (Chl1, Chl2 and Chl3) at Zoujiashan and Yunji. (a) Alkali metasomatic uranium mineralization (early ore stage) at Yunji deposit, the red line is the fracture; (b) alkali metasomatic uranium mineralization (early ore stage) was overprinted with the fluorite-illite alteration (main ore stage) at Zoujishan deposit, the yellow line is the boundary of two styles of alteration; (c) typical high grade uranium ore body at Zoujiashan deposit; (d,e) biotite replaced by chlorite (Chl1-Y and Chl1-Z) in the weakly altered wall rock; (f,g) vein-type Chl2 is intergrown with brannerite or uraninite in alkali metasomatic type ores (Yunji deposit), accompanied by apatite and albite deposition; (h–j) disseminated Chl3 are closely associated with uranium minerals, illite, and fluorite (Zoujiashan deposit). Abbreviations: Pit—pitchblende; Brn—brannerite; Chl—chlorite; Ap—apatite; Ab—albite; Hem—hematite; Kf—potassium feldspar; Flu—fluorite; ill—illite; Zr—zircon.

Likewise, two chlorite types were found at Zoujiashan, i.e., Chl1-Z and Chl3. The pre-ore Chl1-Z is also widespread in the surrounding wall rocks of this deposit and the extension of Chl1-Z alteration could spread over hundreds of meters. Chl1-Z has similar characteristics with pre-ore Chl-Y from Yunji deposit in morphology and genesis. Similarly, Chl1-Z is also derived from partial or complete transformation of the magmatic biotite during the pre-ore stage (Figure 4d). The Chl3 at Zoujiashan is intensively modified or devoid due to the overprinting by later acidic metasomatic alteration (Figure 4b). In contrast to Chl2, the Chl3 is related to acidic metasomatic U-Th mineralization. The disseminated pitchblende, fluorite and illite were commonly intergrown with Chl3 (Figure 4g,h).

4. Sampling and Analytical Methods

In this study, twenty-one ore and wall-rock samples were collected from drill holes and underground mining tunnels at the Zoujiashan and Yunji mining area. The approximate sample locations are shown in Figure 1. For better comparison, the protolith of all samples is porphyritic lava. For the chlorite-bearing or fluorite-bearing samples, more than 50 polished thin sections were prepared for backscattered electron imaging, in-situ EPMA and LA-ICP-MS elemental analyses.

The major element analysis for chlorite was carried out with the JXA-8100 electron microprobe at the Beijing Research Institute of Uranium Geology (BRIUG, CNNC). The operating conditions included accelerated voltage of 20 kV, beam current of 1×10^{-8} A, beam diameter of 1 μm and 0.01% detection limit. Ten to thirty seconds counting time on different peaks were set and the detection limit was 0.002%. The elements measured included Si, Mg, Fe, Al, Na, K, Ca. The standards used include kaersutite for K, Fe and Mg, hornblende for Si and Ca, topaz for Al. The chemical formula of chlorite is calculated based on 14 oxygen atoms per formula unit (a.p.f.u).

The in-situ LA-ICP-MS trace elements for chlorite were performed at the Ore Deposit and Exploration Centre, Hefei University of Technology, Hefei, China. The laser ablation was performed using an Agilent 7900 ICP-MS coupled to a Teledyne Cetac Technologies Analyte HE 193 nm ArF excimer laser. The analysis conditions include a spot diameter of 30 μm , a 10 Hz pulse repetition rate, and an energy density of $4 \text{ J}/\text{cm}^{-2}$. Samples and standards were ablated for 40 s after measuring the gas blank for ~ 20 s. The standards NIST 610, NIST 612, and BCR 2G were utilized as used as the external standards. Aluminium was used as the internal standard for chlorite. A total of 50 chemical elements have been analyzed for the Xiangshan chlorite, including Si, Al, Mg, Fe, Mn, K, Ca, Na, Sc, Ti, V, Cr, Co, Ni, Cu, Zn, Ga, As, Rb, Sr, Y, Zr, Nb, Mo, Cd, Sn, Sb, Ba, La, Ce, Pr, Nd, Sm, Eu, Gd, Tb, Dy, Ho, Er, Tm, Yb, Lu, Hf, Ta, W, Bi, Pb, Th and U. The data reduction was performed using in-house ICPMSDataCal software [53]. The analytical uncertainties were $<10\%$ for most trace element analyses. The detailed procedures are similar to Xiao et al. [4].

5. Results

5.1. Major Elements and Classification of Chlorite

The major and trace element compositions for chlorite determined by EMPA and LA-ICP-MS, are given in Tables S1 and S3, respectively. The chlorite commonly contains mineral inclusions (e.g., uranium minerals) and primary mineral phases (e.g., zircon, apatite) [24]. In the LA-ICP-MS time-resolved signal spectra, most of the elemental signals for chlorite are flat, suggesting that the trace elements are mainly present in the crystal lattice. In addition, to further avoid contamination by other phyllosilicate minerals, chlorite analyses with more than $w(\text{Na}_2\text{O} + \text{K}_2\text{O} + \text{CaO}) > 0.5\%$ were discarded [4]. Accordingly, a total of 92 EPMA spot analyses and 57 LA-ICP-MS spot analyses were validated and selected for discussion.

Overall, chlorite from Zoujishan and Yunji have total value ranging for 85.25% to 93.12%. They show a relatively wide range of SiO_2 and Al_2O_3 contents that vary from 23.73% to 30.48%, and 15.43% to 22.01%, respectively. There is a wide variation in MgO and FeO contents in different types of chlorites due probably to the main substitutions: $\text{Mg}^{2+} \leftrightarrow \text{Fe}^{2+}$. The Chl1 and Chl3 have relatively high FeO contents with average of 36.77% and 40.96%, respectively, but relatively low MgO contents with average of 5.15% and 4.47%, respectively. In contrast, the Chl2 has relatively low FeO content with average of 26.81% but higher MgO content with average of 12.73%. The EPMA results for CaO, K_2O , and Na_2O for all different types of chlorites are uniformly low.

In this study, we also recalculated chlorite EPMA data based on the 14 oxygen atoms per formula unit (a.p.f.u.). In the ternary Al + \square -Mg-Fe diagram (Figure 5b), almost all the data plotted in the Fe-chlorite domain. The Si vs. Fe (a.p.f.u) classification diagram (Figure 5a) indicates that most of Chl1-Y and Chl-Z mainly plotted in/near the brunsvigite domain, whereas Chl2 mainly fall in the pycnochlorite and brunsvigite. Chl3 displays a large compositional variation and mainly scattered across the brunsvigite to daphnite domains.

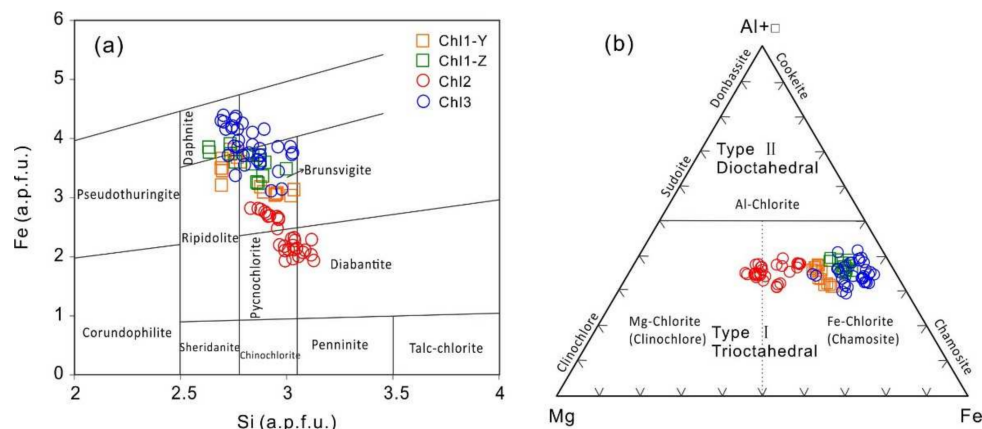


Figure 5. Chlorite classification diagrams at the Zoujiashan deposit and Yunji deposit. (a) Si vs. Fe (a.p.f.u) diagram (after [54]); (b) (Al)–Mg–Fe diagram (after [55]).

5.2. Trace Elements in Chlorite

LA-ICP-MS trace element data for different types of chlorites are presented in Table S3 and illustrated in Figure 6. The contents of Fe, Mg, Si and Al measured by LA-ICP-MS are consistent with those given by EPMA. Certain trace elements of these chlorite (e.g., Mn, Ti, Zn, V, Cr, Ni, Sc, Co, Ga, Sr, Ce, U and Pb) are significantly higher than the detection limits (Figure 7). However, contents of other trace elements (e.g., Be, Cu, Ba, Zr, Nb, Mo, Ag, Sn, Sb, Cs, Ta, Tl, Bi) are nearly below the detection limits. Thus, these elements will not be included in the following discussion.

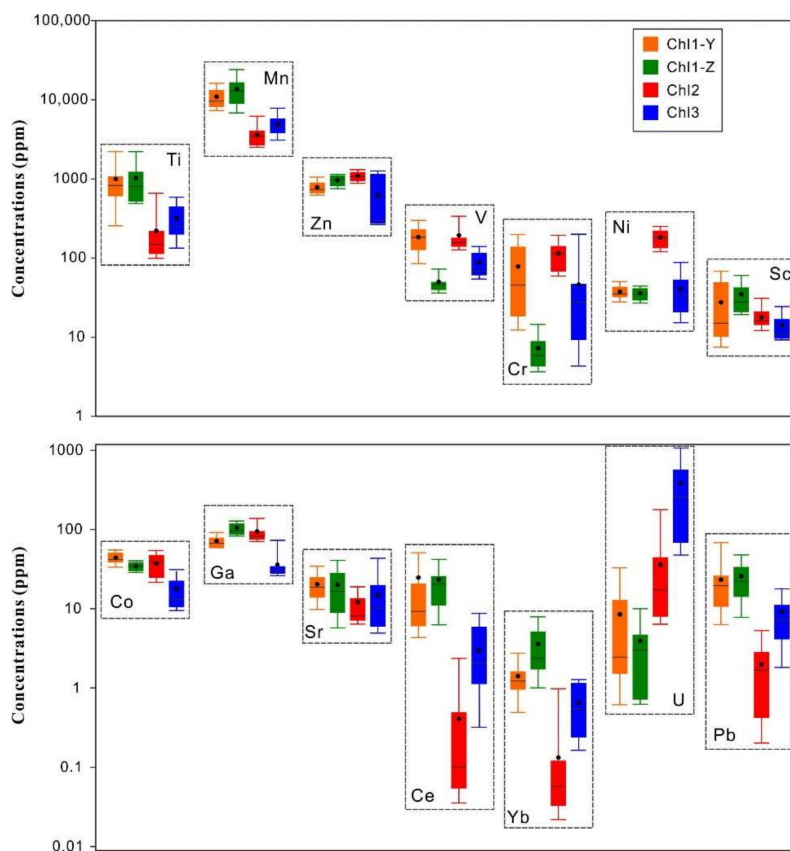


Figure 6. Trace element box plot for chlorite at the Zoujiashan deposit and Yunji deposit.

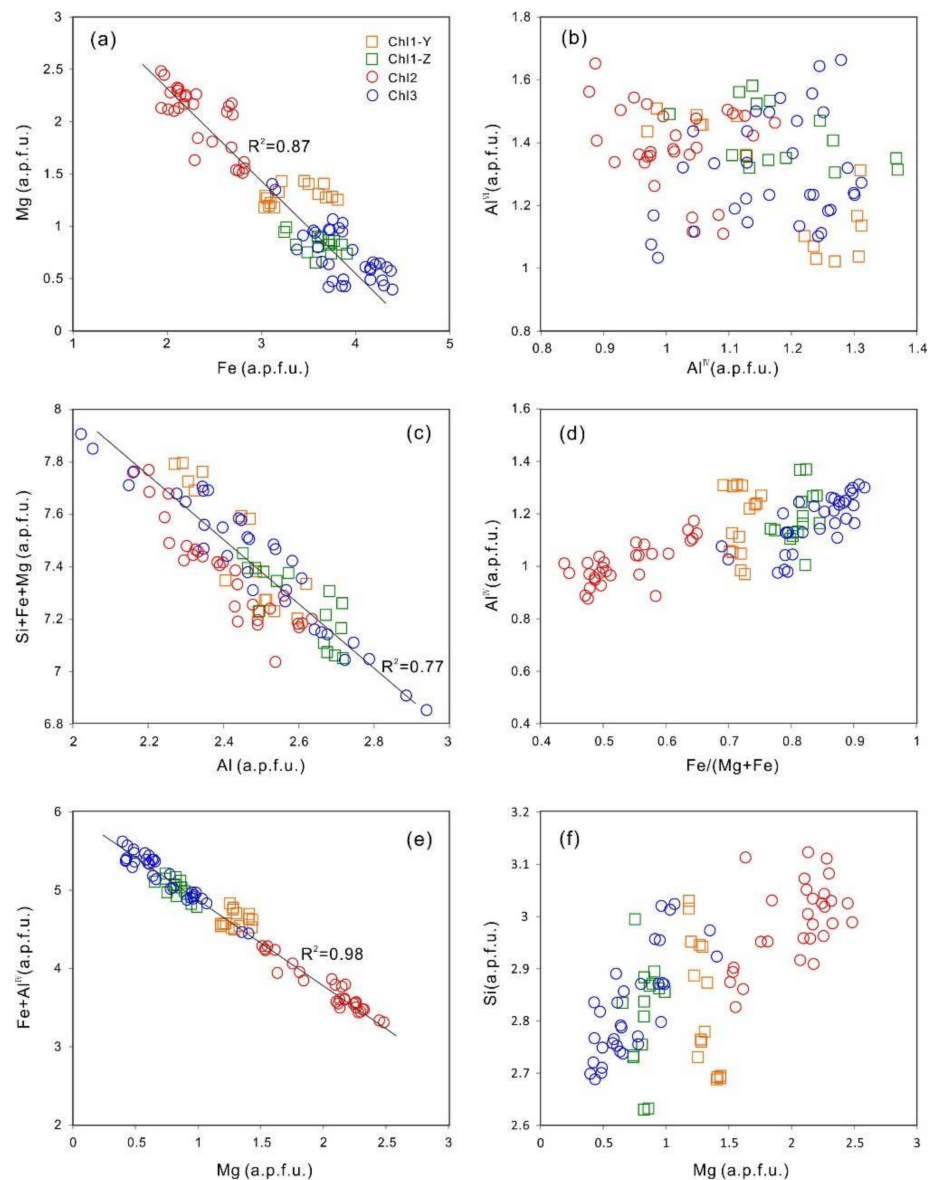


Figure 7. Binary diagram of chlorite at the Zoujiashan deposit and Yunji deposit (calculated based on 14 oxygen atoms, a.p.f.u.) (a) Fe vs. Mg; (b) Al^{VI} vs. Al^{IV}; (c) Al vs. Si + Fe + Mg; (d) Fe/(Mg + Fe) vs. Al^{IV}; (e) Mg vs. Fe + Al; (f) Mg vs. Si.

Manganese is the most abundant trace element in all of these chlorite analyses and generally range from 2000 to 15,000 ppm. The Chl1, Chl2, and Chl3 contain similar high Sr contents (6–37 ppm, 6–44 ppm, and 5–39 ppm). Overall, the pre-ore Chl1-Y have the similar trace element patterns with Chl1-Z except for higher V (130–279 ppm) and Cr (15.5–186 ppm). Compared with the pre-ore chlorite (Chl1-Z and Chl1-Y), the vein-like/disseminated chlorite (Chl2 and Chl3) related to uranium mineralization exhibit markedly distinct trace element trends, such as much lower Ti, Mn, Sc, Rb, REEs and Pb, but pronouncedly higher U and Th (Figure 6 and Table S3). Compared to the Chl2 that formed in the early ore stage, Chl3 is slightly enriched in Ti (140–550 ppm), Mn (3981–6200 ppm), REEs (1.3–21 ppm), U (51–901 ppm) and Pb (1.7–135 ppm), but depleted in Zn (280–1176 ppm), V (63–131 ppm), Cr (5–188 ppm), Ni (16–82 ppm), Sc (9–27 ppm), Co (10–49 ppm), and Ga (30–68 ppm).

6. Discussion

6.1. Elemental Substitution Mechanism of Chlorite

Chlorite group minerals are hydrous phyllosilicates with a wide compositional range, in which Si and Al^{IV} generally occupy the tetrahedral position, whereas Mg, Fe and Al^{VI} occupy the octahedral position [24,56,57]. Three ion substitution mechanisms for chlorite were proposed in the past, i.e., (1) Fe²⁺ \leftrightarrow Mg²⁺, (2) Tschermak Al^{IV} and Al^{VI} \leftrightarrow Si (Mg²⁺, Fe²⁺), and (3) di-trioctahedral 3(Mg²⁺, Fe²⁺) \leftrightarrow □ + 2 Al^{VI} [14]. The substitution mechanism is mainly dependent on the pressure, temperature, chemical compositions of host rock and physicochemical conditions of the hydrothermal environment [24].

As shown in Figure 7a, the Fe (a.p.f.u) has a good negative correlation with Mg (a.p.f.u) ($R^2 = 0.87$), suggesting that the replacement between Mg²⁺ and Fe²⁺ is predominant for ionic substitution in the octahedral position [31]. For all types of chlorites, the Al^{VI} values of Xiangshan chlorite range from 1.031 to 1.664, and the Al^{IV} values range from 0.876 to 1.312. In general, the Al^{VI} values are higher than Al^{IV} in four types of chlorites. In the Al^{IV} vs. Al^{VI} diagram (Figure 7b), the Al^{IV} has no correlation with Al^{VI}, suggesting that the ditrioctahedral substitution (3(Mg²⁺, Fe²⁺) \leftrightarrow □ + 2 Al^{VI}) is likely not that important [26]. The Al_{total} shows a good negative correlation ($R^2 = 0.77$) with (Si + Fe²⁺ + Mg²⁺) value (Figure 7c), indicating the Tschermak substitution at Xiangshan chlorite is prevalent. In the Mg-(Fe + Al^{VI}) diagram (Figure 7e), all of the four types of chlorites show perfectly negative correlation ($R^2 = 0.98$), suggesting that Fe and Al^{VI} predominantly substitute the Mg in the octahedral position. In addition, there is a moderate correlation between Al^{IV} and Fe/(Fe + Mg) in chlorite from the two deposit (Figure 7d), indicating that Fe/(Fe + Mg) ratio has substantial effect on the calculated chlorite formation temperatures which will be discussed later.

6.2. Chlorite Geothermometry

Numerous studies have proven that the formation temperatures of chlorite can be estimated using the chemical composition. Up to now, several empirical formula geothermometers have been proposed and successfully used in different geological environments [1,20,58].

Hey [54] firstly found that there is a qualitative relationship between the polytype of chlorite and its formation temperature. Cathelineau and Nieva [47] studied the relationship between composition and temperature of chlorite at the Los Azufres and Salton Sea geothermal systems in Mexico, and proposed a chlorite geothermometer based on the positive correlation between Al^{IV} in chlorite and the formation temperature. Kranidiotis and MacLean [57] revised Cathelineau's thermometer and further pointed out that the formula is suitable for Al-saturated chlorite. Jowett [58] further modified the thermometer proposed by Kranidiotis and MacLean, and suggested that the premise of the thermometer formula is applicable to the chlorite with n(Fe)/n(Fe + Mg) < 0.6 that formed at a temperature of 150~325 °C in the geothermal system. Stefano [59] used the XRD results to calculate the temperature at which chlorite was formed.

In this study, the Fe/(Fe + Mg) ratio and Al^{IV} shows a good positive correlation (Figure 7d), and the majority of Fe/(Fe + Mg) ratios of Zoujiashan and Yunji chlorite is higher than 0.6 (Table S2). Thus, the contribution of Fe and Mg in the chlorite thermometer cannot be ignored [1,57]. The Al₂O₃ contents of the four types of chlorites generally vary from 16% to 21% (mean = 19.05%), and the Al-rich minerals are absent in the ores, indicating the chlorite at Xiangshan is Al-unsaturated. Therefore, the empirical formulae proposed by Stefano [59] was used to evaluate the chlorite formation temperatures (Figure 8; Table S2), and the calculation formula is: $t(^{\circ}\text{C}) = [14.379 - (d_{001}/0.1 \text{ nm})]/0.001$. The $d_{001}/0.1 \text{ nm}$ value was obtained by the formulae as $d_{001}/0.1 \text{ nm} = 14.339 - 0.115 n(\text{Al}^{\text{IV}}) - 0.0201 n(\text{Fe}^{2+})$ (the structural formula of chlorite in this formula is calculated based on 14 oxygen atoms), which was proposed by Raused-Colom et al. [60] and modified by Nieto [61]. Based on these empirical formulae, the synthetic diagram yielded a wide temperature range of 179~277 °C (Table S2). The calculated temperatures of pre-ore Ch11-Y (214~264 °C, mean = 242 °C) from Yunji are consistent with those of Ch11-Z (225~275 °C, mean = 249 °C).

By contrast, the calculated results of Chl2 (179~231 °C, mean = 203°C) related to alkali metasomatic U mineralization are unequivocally lower than those of Chl3 from Zoujiashan that formed in the acidic metasomatic U mineralization (22~278 °C, mean = 253 °C). Meanwhile, the results for Chl3 are also similar to the fluid-inclusion (FI) homogenization temperatures of quartz and fluorite from Zoujiashan deposit (180–320 °C) [62], whereas the results for Chl2 are consistent with the homogenization temperatures of calcite that is coeval with uranium minerals (120–210 °C, our unpubl. data). Therefore, we suggest that these calculated temperatures can represent the chlorite crystallization temperature at both Zoujiashan deposit and Yunji deposit, since the formation of Chl2 and Chl3 are associated with low-intermediate temperature hydrothermal fluids. The large variation of chlorite crystallization temperatures is probably due to the multi-stage hydrothermal activities.

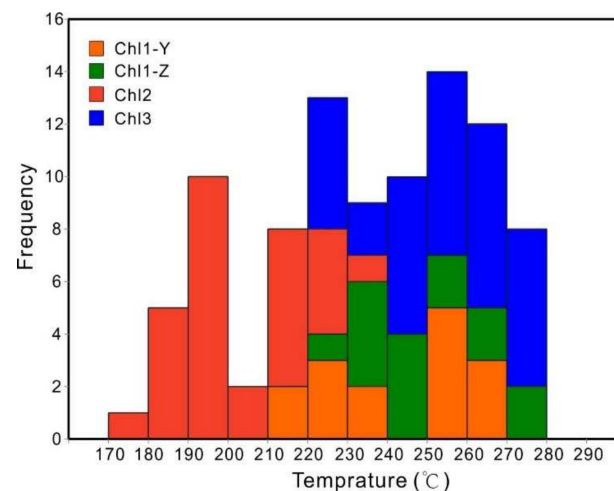


Figure 8. Histogram of the formation temperature range for the Zoujiashan and Yunji chlorite. Empirical geothermometric formula were from [57].

6.3. The Formation Mechanism of Chlorite

As discussed above, the wall rock alteration is very widespread at Zoujiashan and Yunji deposit, especially chloritization and illitization. Through field and microscopic observations, the chlorite is mainly divided into three types based on the occurrences, i.e., (1) replacement-type chlorite (Chl1-Z and Chl1-Y), which partially or completely replaced biotite; (2) disseminated-type chlorite that is (nearly) coeval with uranium minerals; (3) vein-type chlorite in the uranium ores. The replacement-type chlorite (Chl1-Z and Chl1-Y) is formed in the pre-ore stage and commonly has little or no direct links with uranium mineralization, whereas the other two types are closely related to uranium mineralization.

Different mechanisms of chlorite crystallization were reported in previous literature such as solid-state transformation (SST) mechanism, the dissolution–crystallization mechanism (DC mechanism) and the direct precipitation of chlorite from supersaturated solutions [63–65]. In this study, the altered biotite (Chl1-Z and Chl1-Y) basically retained the original morphology and structure (Figure 4d). Thus, the formation mechanism responsible for the replacement-type chlorite is unequivocally dissolution–recrystallization mechanism (DC mechanism). Over the course of pre-ore alteration, the hydrothermal fluid came into contact with the host rock, migrated along the micro fissures of the wall rock or minerals, and further transformed the biotite into chlorite. Almost no Mg and Fe are derived from the hydrothermal fluids. Another very important mechanism resulting in the formation of vein-type and disseminated chlorite at Xiangshan is dissolution–migration–precipitation. Unlike the case for pre-ore chlorite as they are formed via dissolution–precipitation mechanism, the hydrothermal fluids rich in uranium flux might dissolve the rock-forming minerals (i.e., biotite, feldspar) and were directly precipitated as newly formed chlorite after migration for a certain distance. This type of chlorite (Chl2 and Chl3) is closely associated with uranium

mineralization and coexists with pyrite, illite and albite, though they may be formed in different ore stages. As such, a large amount of Fe, Mg and other important trace element in disseminated or vein-type chlorite may be introduced from external fluids.

6.4. Chemical Comparison of the Four Styles of Chlorite at Xiangshan

Chlorite can be formed in many hydrothermal environments and thus exhibits various chemical compositions [3,14]. These compositional variations in chlorite were largely caused by different formation conditions (e.g., temperature–pressure (P–T) and redox state), and fluid and protolith compositions [3,66]. Therefore, in this study, the chemical variation of chlorite formed in different ore stages may reflect the compositional evolution of ore fluids.

The Chl1-Y and Chl1-Z have the similar trace elements contents, such as Ti, Mn, Ce, Ga, Ni, Zn, and U, indicating that they were formed in the same stage, though they occurred in Yunji and Zoujiashan, respectively. This further suggests that the pre-ore hydrothermal fluids forming Chl1-Y and Chl1-Z are characterized by the similar compositions. As illustrated in Figure 6, the replacement-type chlorite samples (Chl1-Y and Chl1-Z) are characterized by relatively high concentrations of Ti, Mn, Rb, some compatible elements (e.g., V, Sc, Co) and rare earth elements, suggesting that this type of chlorite was mainly affected by the protolith and primary mineral compositions rather than the external fluids.

As mentioned above, among the four types of chlorites, the disseminated and vein-type chlorite, i.e., Chl2 and Chl3, are more uranium mineralization-related (Figure 4f–j). However, the Chl3 that formed in the late ore stage has higher FeO and Fe/(Fe + Mg) ratios, whereas Chl2 has higher MgO content. FeO and MgO contents of chlorite were considered to be controlled by primary biotite [5]. Because the protolith that host all types of chlorites from Yunji and Zoujiashan is felsic porphyritic laves in this study, the primary minerals or protolith may not be the main factors responsible for the discrepancy of FeO and MgO contents between Chl2 and Chl3. In addition, the Chl2 and Chl3 commonly coexist with uranium minerals, pyrite, and other newly-formed hydrothermal minerals, indicating that the disseminated or vein-like chlorite was most likely to be directly precipitated from ore-bearing hydrothermal fluids. As such, a reasonable explanation is that the formation conditions (e.g., temperature, pressure) and fluid compositions result in the chemical variations of Chl2 and Chl3. The large difference of calculated formation temperatures for Chl2 and Chl3 confirmed this conjecture. Additionally, the different nature of ore fluids that lead to two episodes of uranium mineralization may therefore influence the compositional variations of newly-formed hydrothermal chlorite. Thus, trace element composition of Chl2 and Chl3 indicate a large distinction. The hydrothermal fluid forming Chl3 is enriched in U, Th, REEs, Mn and Ti, whereas the Chl2 related to alkali metasomatic alteration is more abundant in Zn, Cr, Ni, Ga, and Co (Figure 6).

To conclude, the formation temperatures and fluid chemistry are probably the dominant factor for the compositional discrepancy between the Chl2 and Chl3 that relates to two episodes of uranium mineralization. However, for the replacement-type chlorite (Chl1-Z and Chl1-Y), the differential composition was possibly controlled by the protolith and primary minerals (e.g., biotite), respectively.

6.5. Chlorite Characteristic for Exploration Significance

In this contribution, we focused on two typical uranium deposits in Xiangshan and identified the disseminated- and vein-type chlorite within or proximal to the ore body and replacement-type chlorite in the distal altered country rocks (Figure 4). The samples nearby the ore body are generally characterized by intense chloritization, whereas the distal samples show weak chloritization. As such, the disseminated- and vein-type chlorite presented in proximity to the uranium mineralization can be used as an effective vector toward concealed uranium orebodies. For the majority of uranium deposits in Xiangshan, the alkali metasomatic U mineralization (early ore stage) is widely distributed in the deep part, whereas the acidic metasomatic U mineralization commonly occurs in the upper

part [37,38,45], although the early-ore alteration is often observed to overprint the main-ore alteration zone (Figure 4b). Thus, the presence of Chl3 is an effective indicator toward the most economic (high U grade) mineralized zone at Xiangshan. On the contrary, Chl2 is a vectoring mineral to likely indicate the subeconomic U mineralization and relatively poor uranium exploration at depth.

For porphyry and skarn-related deposits, the chemical compositions of chlorite spatially or temporally exhibit a progressive and continuous trend [3,4,9,14]. These trends were thus used to trace the hydrothermal center or concealed orebodies at depth. However, most analyzed elements of Chl1, Chl2 and Chl3 from Xiangshan do not show such a continuous trend from pre-ore stage to post-ore stage. This is probably because the two episodes of uranium mineralization in Xiangshan were derived from different sources and have significant distinction in ore-forming ages (120–105 Ma and 100–80 Ma, respectively), mineral assemblages and nature of ore fluids [36,37,45]. Nevertheless, compared with the widespread replacement-type chlorite (Chl1), vein-type or disseminated chlorite proximal to the ore body have relatively high U but low Mn, Ti, REEs and Pb contents, which may be used as exploration vectors for the concealed uranium orebodies. Moreover, the Chl3 in the most economical mineralized bodies (main ore stage) commonly have higher U concentration and Fe/(Fe + Mg) ratio. Thus, the Fe/(Fe + Mg) ratio, FeO, MgO, and U contents in chlorite may be regarded as effective geochemical indicators for evaluating the economical mineability of uranium mineralization. Even so, more robust chemical indicators must be further examined by producing more data in the future.

7. Conclusions

(1) At Xiangshan, there are roughly four types of chlorites, i.e., Chl1-Y, Chl1-Z, Chl2 and Chl3. Both Chl1-Y from Yunji and Chl1-Z from Zoujiashan are replacement-type chlorite that are altered from biotite and formed in the pre-ore stage. The pre-ore chlorite is widely distributed in the distal altered country rocks. Chl2 and Chl3 occurs as vein-type/disseminated and are closely related to early-ore U mineralization and main-ore U mineralization, respectively.

(2) The calculated formation temperatures of Chl2 at Yunji and Chl3 at Zoujiashan range from 179 °C to 231 °C and from 221 °C to 278 °C, respectively, which are similar to the homogeneous temperatures of fluid inclusions in calcite of early-ore stage at Yunji and fluorite of main-ore stage at Zoujiashan.

(3) Two important formation mechanisms are responsible for chlorite crystallization at Xiangshan, i.e., dissolution–crystallization mechanism for pre-ore Chl1-Y and Chl1-Z, and dissolution–migration–precipitation mechanism for Chl2 and Chl3.

(4) The compositional difference between Chl2 and Chl3 is mainly controlled by the formation temperatures and fluid compositions/natures. The differential composition of replacement-type chlorite (i.e., Chl1-Z and Chl1-Y) was possibly controlled by the protolith and primary minerals (e.g., biotite, hornblende).

(5) At Xiangshan, the presence of vein-type/disseminated chlorite with high U concentration and Fe/(Fe + Mg) ratio but low Mn, Ti and Pb contents is proximal indicator for the most economic (high U grade) mineralized zone. In contrast, the occurrence of Chl2 is a vectoring mineral to indicate the subeconomic U mineralization and poor uranium exploration at depth.

Supplementary Materials: The following are available online at <https://www.mdpi.com/article/10.3390/min12060693/s1>, Table S1: Electronic probe composition analysis (EPMA) data (wt %), Table S2: Calculated cation numbers of chlorites and recalculated temperatures of Xiangshan chlorite (at standard of 14 oxygen atoms), Table S3: LA-ICP-MS trace elements data of chlorite at Xiangshan (ppm).

Author Contributions: Data curation, W.X.; Funding acquisition, H.F.; Visualization, Y.P.; Writing—original draft, Y.W.; Writing—review and editing, H.F. All authors have read and agreed to the published version of the manuscript.

Funding: The authors received research fellowship from the Basic Research Programs from China National Nuclear Cooperation (D2002), the National Natural Science Foundation (41703042), and the National Key Research and Development Program of China (2017YFC0602600).

Data Availability Statement: The data presented in this study are available in this article.

Acknowledgments: We thank Fangyue Wang for the help with LA-ICP-MS analyses, Xiangkun Ge and Zongyao Tai with EPMA. Jin'an Uranium Co., Ltd. and No. 270 Institute of China National Nuclear Cooperation are extremely appreciated for the assistance during field work. We thank Kunfeng Qiu for his encouragement and support in publishing this research work. We gratefully thank three anonymous reviewers for constructive comments.

Conflicts of Interest: The authors declare that they have no known competing financial interest or personal relationships that could have appeared to influence the work reported in this paper.

References

1. Deer, W.A.; Howie, R.A.; Jussman, J. *Rock-Forming Minerals: Sheet Silicates*; Longman: London, UK, 1962; pp. 1–270.
2. Hayes, J.B. Polytypism of Chlorite in Sedimentary Rocks. *Clays Clayminer.* **1970**, *18*, 285–306. [[CrossRef](#)]
3. Wilkinson, J.J.; Chang, Z.; Cooke, D.R.; Baker, M.J.; Wilkinson, C.C.; Inglis, S.; Gemmell, J.B. The chlorite proximitor: A new tool for detecting porphyry ore deposits. *J. Geochem. Explor.* **2015**, *152*, 10–26. [[CrossRef](#)]
4. Xiao, B.; Chen, H.; Wang, Y.; Han, J.; Xu, C.; Yang, J. Chlorite and epidote chemistry of the Yandong Cu deposit, NW China: Metallogenic and exploration implications for Paleozoic porphyry Cu systems in the Eastern Tianshan. *Ore Geol. Rev.* **2018**, *100*, 168–182. [[CrossRef](#)]
5. Xiao, B.; Chen, H. Elemental behavior during chlorite alteration: New insights from a combined EMPA and LA-ICPMS study in porphyry Cu systems. *Chem. Geol.* **2020**, *543*, 119604. [[CrossRef](#)]
6. Cao, M.J.; Evans, N.J.; Hollings, P.; Cooke, D.R.; McInnes, B.I.A.; Qin, K. Apatite Texture, Composition, and O-Sr-Nd Isotope Signatures Record Magmatic and Hydrothermal Fluid Characteristics at the Black Mountain Porphyry Deposit, Philippines. *Econ. Geol.* **2021**, *116*, 1–20.
7. Cao, M.J.; Hollings, P.; Evans, N.J.; Cooke, D.R.; McInnes, B.I.A.; Zhao, K.D.; Qin, K.Z.; Li, D.F.; Sweet, G. In situ elemental and Sr isotopic characteristics of magmatic to hydrothermal minerals from the Black Mountain porphyry deposit, Baguio District, Philippines. *Econ. Geol.* **2020**, *115*, 927–944. [[CrossRef](#)]
8. Cao, M.J.; Evans, N.J.; Qin, K.Z.; Danišik, M.; Li, G.M.; McInnes, B.I.A. Open Apatite Sr Isotopic System in Low-Temperature Hydrous Regimes. *J. Geophys. Res. Solid Earth* **2019**, *124*, 11192–11203. [[CrossRef](#)]
9. Wang, Z.; Chen, B.; Yan, X.; Li, S. Characteristics of hydrothermal chlorite from the Niujuan Ag-Au-Pb-Zn deposit in the north margin of NCC and implications for exploration tools for ore deposits. *Ore Geol. Rev.* **2018**, *101*, 398–412. [[CrossRef](#)]
10. Qiu, K.F.; Yu, H.C.; Hetherington, C.; Huang, Y.Q.; Yang, T.; Deng, J. Tourmaline composition and boron isotope signature as a tracer of magmatic-hydrothermal processes. *Am. Mineral.* **2021**, *106*, 1033–1044. [[CrossRef](#)]
11. Qiu, K.F.; Yu, H.C.; Deng, J.; McIntire, D.; Gou, Z.Y.; Geng, J.Z.; Chang, Z.S.; Zhu, R.; Li, K.N.; Goldfarb, R.J. The giant Zaozigou orogenic Au-Sb deposit in West Qinling, China: Magmatic or metamorphic origin? *Miner. Depos.* **2020**, *55*, 345–362. [[CrossRef](#)]
12. Qiu, K.F.; Goldfarb, R.J.; Deng, J.; Yu, H.C.; Gou, Z.Y.; Ding, Z.J.; Wang, Z.K.; Li, D.P. Gold deposits of the Jiaodong Peninsula, eastern China. *SEG Spec. Publ.* **2020**, *23*, 753–773.
13. Cao, M.J.; Qin, K.Z.; Evans, N.J.; Li, G.M.; Ling, X.X.; McInnes, B.I.A.; Zhao, J.X. Titanite in situ SIMS U–Pb geochronology, elemental and Nd isotopic signatures record mineralization and fluid characteristics at the Pusanguo skarn deposit, Tibet. *Miner. Depos.* **2021**, *56*, 907–916. [[CrossRef](#)]
14. Zhang, S.; Xiao, B.; Long, X.; Chu, G.; Cheng, J.; Zhang, Y.; Xu, G. Chlorite as an exploration indicator for concealed skarn mineralization: Perspective from the Tonglushan Cu–Au–Fe skarn deposit, Eastern China. *Ore Geol. Rev.* **2020**, *126*, 103778. [[CrossRef](#)]
15. Yu, C.D.; Wang, K.X.; Liu, X.D.; Cuney, M.; Pan, J.Y.; Wang, G.; Zhang, L.; Zhang, J. Uranium mineralogical and chemical features of the Na-metasomatic type uranium deposit in the Longshoushan metallogenic belt, Northwestern China. *Minerals* **2020**, *10*, 335. [[CrossRef](#)]
16. René, M. Alteration of granitoids and uranium mineralization in the Blatná suite of the central Bohemian plutonic complex, Czech Republic. *Minerals* **2020**, *10*, 821. [[CrossRef](#)]
17. Chen, X.; Wen, C.; Meng, D.; Li, B.; Jiang, B.; Qin, J. Implications of major and trace element migration in altered granites for hydrothermal alteration and granite-related uranium mineralization in the Sanjiu ore field, South China. *Minerals* **2022**, *12*, 144. [[CrossRef](#)]
18. Wang, Y.J.; Lin, J.R.; Hu, Z.H.; Wang, F.; Pang, Y.Q.; Gao, F. Characteristics of chlorite from Yunji deposit in Xiangshan uranium orefield and their geological implication. *Uranium Geol.* **2018**, *34*, 153–158. (In Chinese with English Abstract)
19. Wu, D.; Pan, J.; Xia, F.; Huang, G.; Lai, J. The mineral chemistry of chlorites and its relationship with uranium mineralization from Huangsha uranium mining area in the Middle Nanling Range, SE China. *Minerals* **2019**, *9*, 199. [[CrossRef](#)]

20. Lan, Q.; Fu, S.; Lin, J. Characteristics of mineralization-forming fluid and metallogenic mechanism for the Mianhuakeng uranium deposit in South China: Constraints from in situ geochemical signatures and sulfur isotopes of syn-mineralization pyrite and pitchblende. *Minerals* **2022**, *12*, 227. [[CrossRef](#)]
21. Wu, M.Q.; Samson, I.M.; Qiu, K.F.; Zhang, D.H. Concentration mechanisms of REE-Nb-Zr-Be mineralization in the Baerzhe deposit, NE China: Insights from textural and chemical features of amphibole and rare-metal minerals. *Econ. Geol.* **2021**, *116*, 651–679. [[CrossRef](#)]
22. Qiu, K.F.; Yu, H.C.; Wu, M.Q.; Geng, J.Z.; Ge, X.K.; Gou, Z.Y.; Taylor, R.D. Discrete Zr and REE mineralization of the Baerzhe rare-metal deposit, China. *Am. Mineral.* **2019**, *104*, 1487–1502. [[CrossRef](#)]
23. Huang, Y.Q.; Wu, M.Q.; Germain, B.; Yu, H.C.; Qiao, B.X.; Zhao, Z.G.; Qiu, K.F. Geodynamic setting and ore formation of the Younisaiy thorium deposit in the Altyn orogenic belt, NW China. *Ore Geol. Rev.* **2021**, *140*, 104552. [[CrossRef](#)]
24. Inoue, A.; Kurokawa, K.; Hatta, T. Application of chlorite geothermometry to hydrothermal alteration in Toyoha geothermal system, Southwestern Hokkaido, Japan. *Resour. Geol.* **2010**, *60*, 52–70. [[CrossRef](#)]
25. Cathelineau, M.; Nieva, D. A chlorite solid solution geothermometer the Los Azufres (Mexico) geothermal system. *Contrib. Mineral. Petrol.* **1985**, *91*, 235–244. [[CrossRef](#)]
26. Xie, X.; Byerly, G.R.; Ferrell, R.E., Jr. Ilb trioctahedral chlorite from the Barberton greenstone belt: Crystal structure and rock composition constraints with implications to geothermometry. *Contrib. Mineral. Petrol.* **1997**, *126*, 275–291. [[CrossRef](#)]
27. Vidal, O.; Parra, T. Exhumation paths of high-pressure metapelites obtained from local equilibria for chlorite–phengite assemblages. *Geol. J.* **2000**, *35*, 139–161. [[CrossRef](#)]
28. Vidal, O.; Parra, T.; Trotet, F. A thermodynamic model for Fe-Mg aluminous chlorite using data from phase equilibrium experiments and natural pelitic assemblages in the 100 to 600 C, 1 to 25 kb range. *Am. J. Sci.* **2001**, *301*, 557–592. [[CrossRef](#)]
29. Bourdelle, F.; Parra, T.; Chopin, C.A. New Chlorite Geothermometer for Diagenetic to Low-Grade Metamorphic Conditions. *Contrib. Mineral. Petrol.* **2013**, *165*, 723–735. [[CrossRef](#)]
30. Cathelineau, M. Cation site occupancy in chlorites and illites as a function of temperature. *Clay Miner.* **1988**, *23*, 471–485. [[CrossRef](#)]
31. Yavuz, F.; Kumral, M.; Karakaya, N.; Karakaya, M.C.; Yıldırım, D.K. A Windows program for chlorite calculation and classification. *Com. Geosci.* **2015**, *81*, 101–113. [[CrossRef](#)]
32. Walshe, J.L. A six-component chlorite solid solution model and the conditions of chlorite formation in hydrothermal and geothermal systems. *Econ. Geol.* **1986**, *81*, 681–703. [[CrossRef](#)]
33. Halter, W.E.; Webster, J.D. The magmatic to hydrothermal transition and its bearing on ore-forming systems. *Chem. Geol.* **2004**, *210*, 1–6. [[CrossRef](#)]
34. Lanari, P.; Wagner, T.; Vidal, O. A thermodynamic model for di-trioctahedral chlorite from experimental and natural data in the system MgO–FeO–Al₂O₃–SiO₂–H₂O: Applications to P–T sections and geothermometry. *Contrib. Mineral. Petrol.* **2014**, *167*, 1–19. [[CrossRef](#)]
35. OECD/NEA-IAEA. *Uranium 2019, Resources, Production and Demand (The Red Book)*; OECD NEA-IAEA Report: Paris, France, 2020.
36. Bonnetti, C.; Liu, X.; Cuney, M.; Mercadier, J.; Riegler, T.; Yu, C. Evolution of the uranium mineralisation in the Zoujiashan deposit, Xiangshan ore field: Implications for the genesis of volcanic-related hydrothermal U deposits in South China. *Ore Geol. Rev.* **2020**, *122*, 103514. [[CrossRef](#)]
37. Lin, J.R.; Hu, Z.H.; Wang, Y.J.; Zhang, S.; Tao, Y. Ore-forming age and thermal history of uranium-polymetallic mineralization at Xiangshan uranium orefield. *Acta Petrol. Sin.* **2019**, *35*, 193–198. (In Chinese with English Abstract)
38. Hu, B.; Qiu, L.; Li, M.; Sun, Z.; Lv, G.; Zhou, Y.; Bai, L. The tectono-magmatic evolution and metallogenic regularity of Xiangshan uranium ore-field in Jiangxi Province. *Earth Sci. Front.* **2015**, *22*, 29–36. (In Chinese with English Abstract)
39. Yu, X.Q.; Wu, G.G.; Shu, L.S.; Yan, T.Z.; Zhang, D.; Di, Y.J. The Cretaceous tectonism of the Gan-Hang Tectonic Belt, southeastern China. *Earth Sci. Front.* **2006**, *13*, 31–43. (In Chinese with English Abstract)
40. Dahlkamp, J.F. *Uranium Deposits of the World*; Springer: Berlin/Heidelberg, Germany, 2009; pp. 86–157.
41. Mao, J.W.; Pirajno, F.; Cook, N. Mesozoic metallogeny in East China and corresponding geodynamic settings—An introduction to the special issue. *Ore Geol. Rev.* **2011**, *43*, 1–7. [[CrossRef](#)]
42. Gilder, S.A.; Keller, G.R.; Luo, M.; Goodell, P.C. Eastern Asia and the Western Pacific timing and spatial distribution of rifting in China. *Tectonophysics* **1991**, *197*, 225–243. [[CrossRef](#)]
43. Zhou, X.M.; Sun, T.; Shen, W.Z.; Shu, L.S.; Niu, Y.L. Petrogenesis of Mesozoic granitoids and volcanic rocks in South China: A response to tectonic evolution. *Episodes* **2006**, *29*, 26–33. [[CrossRef](#)]
44. Qin, K.Z.; Zhai, M.G.; Li, G.M.; Zhao, J.X.; Zeng, Q.D.; Gao, J.; Xiao, W.J.; Li, J.L.; Sun, S. Links of collage orogenesis of multiblocks and crust evolution to characteristic metallogenesis in China. *Acta Petrol. Sin.* **2017**, *33*, 305–325. (In Chinese with English Abstract)
45. Fan, H.H.; Ling, H.F.; Wang, D.Z.; Liu, C.S.; Shen, W.Z.; Jiang, Y.H. Study on metallogenetic mechanism of Xiangshan uranium ore-field. *Uranium Geol.* **2003**, *19*, 208–213. (In Chinese with English Abstract)
46. Jiang, Y.H.; Ling, H.F.; Jiang, S.Y.; Shen, W.Z.; Fan, H.H.; Ni, P. Petrogenesis of a Late Jurassic peraluminous volcanic complex and its high-Mg, potassic, quenched enclaves at Xiangshan, Southeast China. *J. Petrol.* **2005**, *46*, 1121–1154. [[CrossRef](#)]

47. Wang, Y.J.; Nie, J.T.; Lin, J.R.; Wang, H.Z. Geochronology and geochemistry of the felsic-intermediate dikes from Xiangshan uranium ore field, South China: Implications for petrogenesis, tectonic setting and uranium mineralization. *Mineral. Petrol.* **2022**. [[CrossRef](#)]
48. Wang, Y.J.; Lin, J.R.; Hu, Z.H.; Dong, Q.; Liu, R.P.; Pang, Y.Q.; Gao, F.; Tao, Y. Zircon U-Pb geochronology, geochemistry and Hf isotopic compositions of dacitic porphyry in Zoujiashan deposit of Xiangshan uranium orefield and its geological implication. *Earth Sci.* **2021**, *46*, 31–42. (In Chinese with English Abstract)
49. Yang, S.Y.; Jiang, S.Y.; Jiang, Y.H.; Zhao, K.D. Geochemical constraints on zircon U-Pb dating and Sr-Nd-Hf isotopic the age and petrogenesis of an early Cretaceous volcanic-intrusive complex at Xiangshan, Southeast China. *Miner. Petrol.* **2011**, *101*, 21–48. [[CrossRef](#)]
50. Chen, Z.L.; Han, F.S.; Yang, N.; Wang, Y. Topographic erosive diversities of the Xiangshan uranium orefield and its implications for preservation: Evidences from fission track dating of apatite. *Chin. J. Geophys.* **2013**, *55*, 2371–2384. (In Chinese with English Abstract)
51. Jiang, Y.H.; Ling, H.F.; Jiang, S.Y.; Shen, W.Z.; Fan, H.H.; Ni, P. Trace element and Sr-Nd isotope geochemistry of fluorite from the Xiangshan uranium deposit, southeast China. *Econ. Geol.* **2006**, *101*, 1613–1622. [[CrossRef](#)]
52. CNG (China Nuclear Geology); BRIUG (Beijing Research Institute of Uranium Geology). *The Research and Evaluation of Volcanic-Related Uranium Deposit in China*; China National Nuclear Corporation: Beijing, China, 2010; pp. 814–935. (In Chinese)
53. Liu, Y.; Hu, Z.; Gao, S.; Günther, D.; Xu, J.; Gao, C.; Chen, H. In situ analysis of major and trace elements of anhydrous minerals by LA-ICP-MS without applying an internal standard. *Chem. Geol.* **2008**, *257*, 34–43. [[CrossRef](#)]
54. Hey, M.H. A new review of the chlorites. *Mineral. Mag. J. Mineral. Soc.* **1954**, *30*, 277–292. [[CrossRef](#)]
55. Zane, A.; Weiss, Z. A procedure for classifying rock-forming chlorites based on microprobe data. *Rend. Lincei* **1998**, *9*, 51–56. [[CrossRef](#)]
56. Wiewióra, A.; Weiss, Z. Crystallochemical classifications of phyllosilicates based on the unified system of projection of chemical composition: II. The chlorite group. *Clay Miner.* **1990**, *25*, 83–92. [[CrossRef](#)]
57. Kranidiotis, P.; MacLean, W.H. Systematics of chlorite alteration at the Phelps Dodge massive sulfide deposit, Matagami, Quebec. *Econ. Geol.* **1987**, *82*, 1898–1911. [[CrossRef](#)]
58. Jowett, C. Fitting iron and magnesium into the hydrothermal chlorite geothermometer. *SSRN* **2021**, 3863523. [[CrossRef](#)]
59. Stefano, B. Applying X ray geothermometer diffraction to a chlorite. *Clays Clay Miner.* **1999**, *47*, 54–63.
60. Raused-Colom, J.A.; Wiewiora, A.; Matesanz, E. Relationship between composition and d001 for chlorite. *Am. Mineral.* **1991**, *76*, 1373–1379.
61. Niet, F. Chemical composition of metapelite chlorites: X-ray diffraction and optical property approach. *Eur. J. Mineral.* **1997**, *9*, 829–841. [[CrossRef](#)]
62. Guo, J.J.; Qiu, L.F.; Hu, B.Q.; Gao, H.D.; Wang, Y.X. Characteristics of fluid inclusions of the ultra-rich ore from Zoujiashan uranium deposit at Xiangshan orefield of Jiangxi, China: Insights from paragenesis apatite-purple black fine crystal fluorite and other minerals. *J. Earth Sci. Environ.* **2020**, *42*, 526–539. (In Chinese with English Abstract)
63. Simmons, S.F.; Browne, P.R. Hydrothermal minerals and precious metals in the Broadlands-Ohaaki geothermal system: Implications for understanding low-sulfidation epithermal environments. *Econ. Geol.* **2000**, *95*, 971–999. [[CrossRef](#)]
64. Beaufort, D.; Rigault, C.; Billon, S.; Billault, V.; Inoue, A.; Inoué, S.; Ferrage, E. Chlorite and chloritization processes through mixed-layer mineral series in low-temperature geological systems—a review. *Clay Miner.* **2015**, *50*, 497–523. [[CrossRef](#)]
65. Pant, S.; Singh, S.; Sahoo, P.R.; Kumar, A.; Saravanan, B.; Venkatesh, A.S.; Kumar, P. Mineral chemistry and geothermometry of chlorites in relation to physico-chemical conditions of uranium mineralization in the central part of the Singhbhum Shear Zone, eastern India. *Ore Geol. Rev.* **2019**, *112*, 102997. [[CrossRef](#)]
66. Kameda, J.; Ujiie, K.; Yamaguchi, A.; Kimura, G. Smectite to chlorite conversion by frictional heating along a subduction thrust. *Earth Planet. Sci. Lett.* **2011**, *305*, 161–217. [[CrossRef](#)]